Surfactant-assisted hydrothermal synthesis of $NaTaO_3$ nanotubes with enhanced photodegradation activity

Haixia Hu[1] ✉, *Yaqin Fu*[2]

[1]*Zhejiang Industry Polytechnic College, Shaoxing 312000, People's Republic of China*
[2]*Key Laboratory of Advanced Textile Materials and Manufacturing Technology of Ministry of Education, Zhejiang Sci-Tech University, Hangzhou 310018, People's Republic of China*
✉ *E-mail: 15167019298@163.com*

Published in Micro & Nano Letters; Received on 10th June 2019; Revised on 13th November 2019; Accepted on 17th January 2020

The morphology of photocatalysts plays an important role in their photocatalytic activity. Here, a novel sodium tantalum trioxide ($NaTaO_3$) nanotube photocatalyst was hydrothermally synthesised with the assistant of Na dodecyl sulphate (SDS) surfactant. The as-synthesised $NaTaO_3$ nanotubes presented an enhanced light absorption, compared with $NaTaO_3$ nanocubes prepared without the addition of SDS. By using rhodamine B (RhB) as organic pollutants model, the $NaTaO_3$ nanotubes exhibited a 96.2% of photodegradation ratio after 80 min ultraviolet light irradiation, which was much higher than $NaTaO_3$ nanocubes and commercial P25. The cycle degradation results revealed that $NaTaO_3$ nanotubes had an excellent photochemical stability. The active species trapping experiment suggested that the dominating active species were hydroxyl radicals and superoxide radicals, rather than holes.

1. Introduction: In consideration of environmental pollution and energy shortage, semiconductor photocatalysis receives increasing attention in recent years [1–3]. The semiconductors can convert renewable light energy to chemical energy under the light irradiation, which provides a fascinating approach to eliminate the organic pollutants of wastewater. Many organic pollutants can be photodegraded successfully to safer end products such as water (H_2O), carbon dioxide (CO_2) and mineral acids via semiconductor photocatalysis [4–6]. However, many photocatalysts reported have a dissatisfactory photocatalytic efficiency in the degradation of organic pollutants due to their inherent features such as high photogenerated holes–electron pair recombination, low redox ability and serious photocorrosion [7–9].

As a new type of ternary oxide semiconductor, NaTa oxide ($Na_xTa_yO_z$) has attracted great attention in photocatalysis application such as photodegradation of organic pollutions, hydrogen evolution and water splitting [10–12]. Jiang group reported that the pyrochlore-like $Na_2Ta_2O_6$ nanocubes with a wide bandgap (~4.6 eV) exhibited an outstanding photocatalytic property under ultraviolet (UV) irradiation [13]. Li group prepared a perovskite-type NaTa trioxide ($NaTaO_3$) nanocube by the hydrothermal method. They found that, compared with pyrochlore-like $Na_2Ta_2O_6$ nanocubes, the perovskite-type $NaTaO_3$ nanocubes possess a narrower bandgap (~4.0 eV), as well as a higher H_2 evolution ability under UV illumination [14]. The higher activity indicated that the perovskite-type $NaTaO_3$ is a promising catalyst in photocatalysis application. Therefore, enhancing photocatalytic activity of $NaTaO_3$ is of great significance. The morphology of photocatalyst is an important factor in photocatalytic property. For example, different morphologies of $Na_2Ta_2O_6$ nanocrystalline prepared by adjusting Na hydroxide (NaOH) concentration presented an obvious difference in photocatalytic activity [15]. Controlling the morphology of $NaTaO_3$ can improve its photocatalytic activity. Some publications indicated that tubular nanophotocatalysts showed better photocatalytic activity, compared with other morphologies such as nanowires and nanocubes [16]. Up to now, $NaTaO_3$ nanocubes, nanoparticles have been synthesised, but the tubular $NaTaO_3$ has never been reported.

Herein, novel $NaTaO_3$ nanotubes were prepared by surfactant-assisted hydrothermal approach, and the optical property and photocatalytic activity of $NaTaO_3$ nanotubes were investigated.

2. Experiments: Ta pentoxide (Ta_2O_5), NaOH, Na dodecyl sulphate (SDS) and absolute ethyl alcohol (CH_3CH_2OH) were purchased from Sinopharm Chemical Reagent Co. Ltd. (Shanghai, China) and were used without further purification.

The $NaTaO_3$ nanotubes were synthesised as follows: 0.442 g Ta_2O_5, 0.08 g NaOH and 0.1 g SDS were dissolved in 37.5 ml of CH_3CH_2OH with magnetic stirring. After 30 min, the solution was transferred in a 50 ml teflon-lined stainless steel autoclave and kept at 180°C for 24 h. After cooled to room temperature, the mixture solution was centrifuged and washed with deionised water and absolute ethanol three times successively. Finally, the products were obtained by drying the wet powders at 60°C for 12 h. $NaTaO_3$ nanocubes were synthesised with the same procedure, just without the addition of SDS.

The morphologies of the as-prepared samples were investigated by S-4800 field-emission scanning electron microscopy (FE-SEM, Hitachi) and crystal structure of samples was analysed with a SIEMENS Diffraktometer D5000 X-ray diffractometer using copper Kα radiation source. X-ray photoelectron spectroscopy (XPS) data were obtained with an ESCALab220i-XL electron spectrometer from VG Scientific using 300 W AlKα radiation. The Brunauer–Emmet–Teller (BET) specific surface area of the samples was determined by a high-speed automated area and pore size analyser (3H-2000PS1). UV–visible (UV–vis) diffuse reflectance spectra were recorded with a UV–vis spectrometer (U-3010, Hitachi).

The photocatalytic activity of the as-prepared $NaTaO_3$ catalysts was evaluated by the photodegradation of RhB (an organic pollutant model). In each experiment, 0.015 g catalysts were dispersed in 50 ml of RhB aqueous solution (10 mg l^{-1}). The irradiation was performed with a 300 W mercury lamp. The change of RhB concentrations (C) in accordance with the irradiation time was measured by JH752 UV–vis spectrophotometer ($\lambda = 552$ nm, Shanghai Jinghua Instruments Co., Ltd.).

3. Results and discussion: $NaTaO_3$ nanoparticles were synthesised by a facile hydrothermal method (reaction equation: $Ta_2O_5 + 2Na^+ + 2OH^- = 2NaTaO_3 + H_2O$), and SDS surfactant were added to regulate the morphology of $NaTaO_3$ nanoparticles. The regular $NaTaO_3$ nanocubes were obtained without SDS surfactant (Fig. 1*a*), whereas $NaTaO_3$ nanotubes with a length of about

© The Institution of Engineering and Technology 2020

doi: 10.1049/mnl.2019.0380

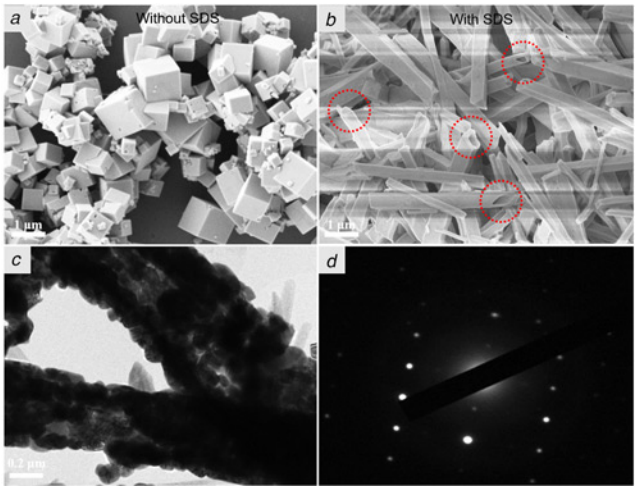


Fig. 1 *SEM images of*
a $NaTaO_3$ nanocubes
b Nanotubes
c TEM image
d SAED pattern of $NaTaO_3$ nanotubes

4 μm were synthesised under the presence of SDS (Fig. 1*b*). The transmission electron microscopy (TEM) image (Fig. 1*c*) indicated that the diameter of the as-synthesised $NaTaO_3$ nanotubes is about 0.5 μm. Moreover, the selected area electron diffraction (SAED, Fig. 1*d*) indicated the single-crystalline nature of $NaTiO_3$ nanotubes.

The addition of SDS surfactant induces a change of $NaTaO_3$ morphology, maybe attributed to the guiding role of SDS and dissolution/recrystallisation mechanism [9, 17]. At the earlier reaction times, the long-chain SDS could guide the oriented growth of $NaTaO_3$ crystal nucleus along the long-chain direction (Fig. 2). With the prolonging of reaction times, the centre of crystals would dissolve gradually due to supersaturation, which recrystallisation proceeded, and the $NaTaO_3$ nanotubes were formed [18]. The growth of $NaTaO_3$ crystal nucleus will be non-directional without SDS.

Fig. 3*a* exhibits the XPS spectrum of the as-synthesised $NaTaO_3$ nanotubes. All component elements of $NaTaO_3$ including Na, Ta and O elements, were found in $NaTaO_3$ nanotubes and the appearance of C element was attributed to CO_2 of the analysis chamber [19]. In XPS spectrum, the peaks at binding energies of 25.1, 529.1 and 1070.1 eV could be assigned to Ta ($4f_{5/2}$), O 1s and Na 1s of $NaTaO_3$, respectively [20]. Fig. 3*b* shows the XRD pattern of the as-prepared $NaTaO_3$ nanotubes. It can be seen that all diffraction peaks of the nanotube sample can be well-indexed to the orthorhombic phase of $NaTaO_3$ (PDF card: 25–0863) and the strong diffraction peaks at $2\theta = 22.9°$ and 32.5° are indexed to (020) and (200) planes of $NaTaO_3$ crystal. The broad peak

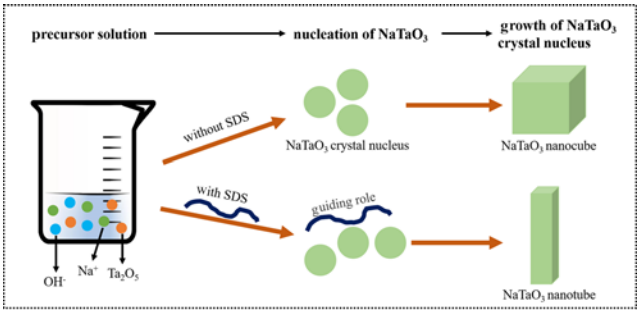


Fig. 2 *Synthetic process of $NaTaO_3$ nanoparticles*

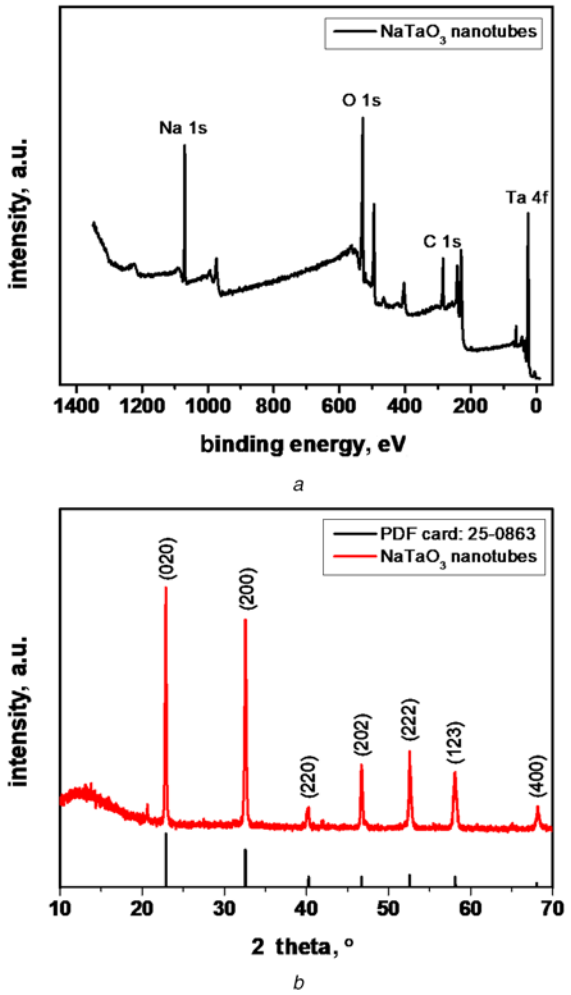


Fig. 3 *XPS spectrum of the as-synthesised $NaTaO_3$ nanotubes*
a XPS spectrum of $NaTaO_3$ nanotubes
b XRD patterns of $NaTaO_3$ nanotubes

of XRD pattern in the region from 10° to 20° can be ascribed to Sodium Tantalum Oxide Hydrate ($H_2(H_2O)Na_2Ta_2O_6$) impurity [10]. Moreover, sharp diffraction peaks in the XRD pattern also indicates a good crystallinity of $NaTaO_3$ nanotubes.

The optical properties of $NaTaO_3$ nanotubes have been tested by UV–vis diffuse reflectance spectroscopy, and the results are shown in Fig. 4*a*. An obvious red shift is observed in $NaTaO_3$ nanotubes. Compared to $NaTaO_3$ nanocubes (330 nm), the absorption edge of $NaTaO_3$ nanotubes is significantly improved, reaching up to 353 nm, implying the enhanced absorption capacity of UV light in $NaTaO_3$ nanotubes. For a crystalline semiconductor, the relationship between optical absorption edge and bandgap can be expressed as follows: $\alpha h\nu = A(h\nu - E_g)^{n/2}$, where α, A, ν, n and E_g represent the absorption coefficient, constant, incident light frequency, bandgap and an integer, respectively [21]. As a kind of direct-gap semiconductor, n value of $NaTaO_3$ is 1 [10]. On the basis of this equation, the bandgaps (E_g) of the $NaTaO_3$ nanocubes and nanotubes were estimated to be 3.79 and 3.54 eV, respectively. The change of bandgaps could be attributed to morphological difference, and hollow structure of $NaTaO_3$ nanotubes can allow multiple reflections of UV light, which enhances light adsorption capacity [22, 23]. The specific surface area of nanoparticles plays an important role in adsorption of organic matter [24]. Therefore, the specific surface area of $NaTaO_3$ nanoparticles was measured by N_2 absorption analysis. As shown in Fig. 4*b*, the BET specific surface areas of $NaTaO_3$ nanocubes and nanotubes were determined to be 32.3 and 59.2 m^2/g, respectively, and the corresponding average pore

© The Institution of Engineering and Technology 2020

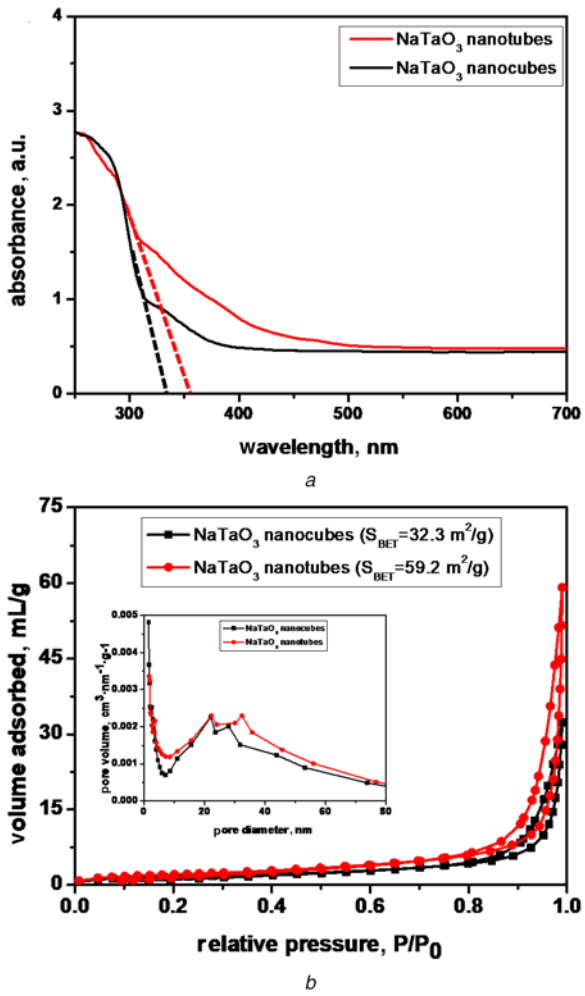


Fig. 4 *Optical properties of $NaTaO_3$ nanotubes*
a UV–vis diffuse spectrum of $NaTaO_3$ nanotubes
b N_2 absorption–desorption isotherm curves of $NaTaO_3$ nanotubes

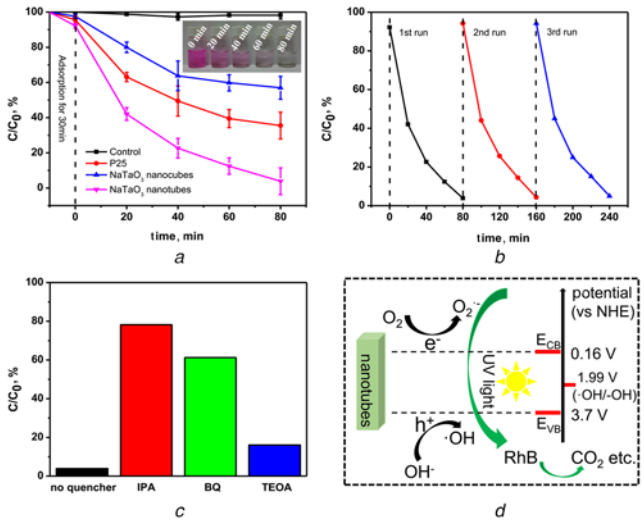


Fig. 5 *Photodegradation of RhB aqueous solution*
a Over different samples
b Cycling runs of $NaTaO_3$ nanotubes
c Trapping experiments of active species during the photocatalytic reaction
d Photocatalytic mechanism scheme of $NaTaO_3$ nanotubes

sizes were centred at 21.27 and 23.41 nm (the inset of Fig. 4*b*). About 83.3% of enhancement ratio in BET specific surface area was ascribed to the hollow structure of $NaTaO_3$ nanotubes.

To investigate the photocatalytic activity of $NaTaO_3$ nanoparticles, the photodegradation of RhB aqueous solution was performed over different samples. As shown in Fig. 5*a*, the self-degradation of RhB with 1.8% of the degradation rate is negligible (control group). When the $NaTaO_3$ nanotubes are used as catalyst, it can be found that the degradation rate of RhB can reach up to 96.2% after 80 min UV light irradiation, which is much higher than $NaTaO_3$ nanocubes (43.1%) and P25 (64.5%). This maybe attributed to the better light absorption ability and higher specific surface area, as demonstrated in Fig. 4. Moreover, the photocatalytic activity of the $NaTaO_3$ nanotubes do not show a significant loss after three recycles (Fig. 5*b*), which indicates that the $NaTaO_3$ nanotubes are photochemically stable in aqueous solution. For exploring the active species of $NaTaO_3$ nanotubes during photodegradation of RhB, holes (h^+), hydroxyl radicals (•OH) and superoxide radical ($O_2^{\bullet-}$) are detected by adding 1.0 mM Triethanolamine (TEOA) (a quencher of h^+), Isopropanol (IPA) (a quencher of •OH) and p-benzoquinone (BQ) (a quencher of $O_2^{\bullet-}$), respectively [25]. After 80 min UV light irradiation, the residual RhB concentration is still 78.2% with the addition of IPA or 61.3% with the addition of BQ (Fig. 5*c*), whereas residual RhB concentration is just 16% with the addition of TEOA. Therefore, it can be determined that the main active species of $NaTaO_3$ nanotubes are •OH and $O_2^{\bullet-}$, rather than h^+. This maybe attributed to the strong reactive activity of •OH and $O_2^{\bullet-}$ [26]. Fig. 5*d* illustrates the plausible photodegradation mechanism of RhB. During UV light irradiation, the electrons of $NaTaO_3$ nanotubes are activated, which forms strong reductive electrons (e^-) at the edge of conduction band (CB) and oxidative holes (h^+) at the edge of valence band (VB). For a semiconductor, the edge potentials of CB (E_{CB}) and VB (E_{VB}) can be calculated with Mulliken electronegativity method: $E_{CB}=\chi-E_e-0.5E_g$, $E_{VB}=E_{CB}+E_g$, where χ is the geometric mean of the Mulliken electronegativity of the constituent atoms; E_e is the free electron energy on the hydrogen scale (about 4.5 eV); and E_g is the bandgap energy of semiconductor [27]. The Mulliken electronegativities of Na, Ta and O atoms are 2.84, 4.34 and 9.62 eV, respectively [28]. The E_{CB} and E_{VB} are, therefore, determined to be 0.16 and 3.7 eV, respectively. The –OH in aqueous solution can be oxidised to •OH (–OH/•OH = 1.99 eV), and the dissolved O_2 will form oxidative $O_2^{\bullet-}$ after the capture of electrons. Under the actions of •OH and $O_2^{\bullet-}$, RhB can be degraded to small-molecule substances such as CO_2.

4. Conclusions: The $NaTaO_3$ nanotubes were hydrothermally synthesised with the assistance of SDS surfactant. Compared to $NaTaO_3$ nanocubes prepared without SDS, the UV light absorption capacity and BET specific surface area of $NaTaO_3$ nanotubes were significantly enhanced. As a result, $NaTaO_3$ nanotubes exhibited excellent photocatalytic activity, with a 96.2% of degradation rate of RhB, much higher than that of $NaTaO_3$ nanocubes and P25. Moreover, The $NaTaO_3$ photocatalysts also exhibited a superior chemical stability. The trapping experiment of active species suggested that the superoxide radical and hydroxyl radicals were the main active species.

5. Acknowledgment: This work was financially supported by the Natural Science Foundation of Zhejiang Province (grant no. Y406310).

6 References

[1] Bag S., Trikalitis P.N., Chupas P.J., *ET AL.*: 'Porous semiconducting gels and aerogels from chalcogenide clusters', *Science*, 2007, **317**, (5837), pp. 490–493

© The Institution of Engineering and Technology 2020

doi: 10.1049/mnl.2019.0380

[2] Kubacka A., Fernández-García M., Colón G.: 'Advanced nanoarchitectures for solar photocatalytic applications', *Chem. Rev.*, 2012, **112**, (3), pp. 1555–1614
[3] Marin M.L., Santos-Juanes L., Arques A., *ET AL.*: 'Organic photocatalysts for the oxidation of pollutants and model compounds', *Chem. Rev.*, 2012, **112**, (3), pp. 1710–1750
[4] Tang B.L., Jiang G.H., Wei Z., *ET AL.*: 'Preparation of N-doped Bi_2WO_6 microspheres for efficient visible-light-induced photocatalysis', *Acta Metall. Sin. (Engl. Lett.)*, 2014, **27**, (1), pp. 124–130
[5] Chatterjee D., Mahata A.: 'Visible-light-induced photodegradation of organic pollutants on dye adsorbed TiO_2 surface', *J. Photochem. Photobiol. A, Chem.*, 2002, **153**, pp. 199–204
[6] Atabaev T.S.: 'Facile hydrothermal synthesis of flower-like hematite microstructure with high photocatalytic properties', *J. Adv. Ceram.*, 2015, **4**, (1), pp. 61–64
[7] Wang R.J., Jiang G.H., Ding Y.W., *ET AL.*: 'Photocatalytic activity of heterostructures based on TiO_2 and halloysite nanotubes', *ACS Appl. Mater. Interfaces*, 2011, **3**, (10), pp. 4154–4158
[8] Zhang L, He Y.M., Wu Y., *ET AL.*: 'Photocatalytic degradation of RhB over $MgFe_2O_4/TiO_2$ composite materials', *Mater. Sci. Eng. B*, 2011, **176**, (18), pp. 1497–1504
[9] Samadipakchin P., Mortaheb H.R., Alireza Z.: 'ZnO nanotubes: preparation and photocatalytic performance evaluation'. *J. Photochem. Photobiol. A.*, 2017, **377**, (15), pp. 91–99
[10] Li X., Zang J.L.: 'Facile hydrothermal synthesis of sodium tantalate ($NaTaO_3$) nanocubes and high photocatalytic properties', *J. Phys. Chem. C*, 2009, **113**, (45), pp. 19411–19418
[11] Lee Y., Watanabe T., Takata T., *ET AL.*: 'Hydrothermal synthesis of fine $NaTaO_3$ powder as a highly efficient photocatalyst for overall water splitting', *ChemInform*, 2007, **38**, (21), pp. 423–428
[12] Kanhere P., Tang Y.X., Zheng J.W., *ET AL.*: 'Synthesis, photophysical properties, and photocatalytic applications of bi-doped $NaTaO_3$ and bi-doped $Na_2Ta_2O_6$ nanoparticles', *J. Phys. Chem. Solids*, 2013, **74**, (12), pp. 1708–1713
[13] Jiang Q.S., Gao J., Yuan H.F., *ET AL.*: 'One-pot, low-temperature preparation of pyrochlore-like $Na_2Ta_2O_6$ nanocrystals by solvothermal synthesis', *Key Eng. Mater.*, 2016, **703**, pp. 267–272
[14] Shi J.Y., Liu G.J., Wang N., *ET AL.*: 'Microwave-assisted hydrothermal synthesis of perovskite $NaTaO_3$ nanocrystals and their photocatalytic properties', *J. Mater. Chem.*, 2012, **22**, (36), pp. 18808–18813
[15] Wang T.T., Lang J.Y., Zhao Y.J., *ET AL.*: 'Simultaneous doping and heterojunction of silver on $Na_2Ta_2O_6$ nanoparticles for visible-light-driven photocatalysis: the relationship between tunable optical absorption, defect chemistry and photocatalytic activity', *CrystEngComm*, 2015, **17**, (35), pp. 6651–6660
[16] Shi L., Yin P.Q., Dai Y.M., 'Synthesis and photocatalytic performance of $ZnIn_2S_4$ nanotubes and nanowires', *Langmuir*, 2013, **29**, (41), pp. 12818–12822
[17] Vaidya S., Rastogi P., Narayan S., *ET AL.*: 'Nanospheres, nanocubes, and nanorods of nickel oxalate: control of shape and size by surfactant and solvent', *J. Phys. Chem. C*, 2008, **112**, (33), pp. 12610–12615
[18] Sun Y., Riley D.J., Ashfold M.N.: 'Mechanism of ZnO nanotube growth by hydrothermal methods on ZnO film-coated Si substrates', *J. Phys. Chem. B*, 2006, **110**, (31), pp. 15186–15192
[19] Tang B.L., Zhang B., Zhuang J.J., *ET AL.*: 'Surface potential governed cellular osteogenic differentiation on ferroelectric polyvinylidene fluoride trifluoroethylene films', *Acta Biomater*, 2018, **74**, pp. 291–301
[20] Wang J.Q., Su S.Y., Liu B., *ET AL.*: 'One-pot, low-temperature synthesis of self-doped $NaTaO_3$ nanoclusters for visible-light-driven photocatalysis', *Chem. Commun.*, 2013, **49**, (71), pp. 7830–7832
[21] Butler M.A.: 'Photoelectrolysis and physical properties of the semiconducting electrode WO_2', *J. Appl. Phys.*, 1977, **48**, (5), pp. 1914–1920
[22] Tian G.H., Chen Y.J, Fu H.G., *ET AL.*: '3D hierarchical flower-like TiO_2 nanostructure: morphology control and its photocatalytic property', *CrystEngComm*, 2011, **13**, pp. 2994–3000
[23] Li H.X., Bian Z.F., Lu Y.F.: 'Mesoporous titania spheres with tunable chamber structure and enhanced photocatalytic activity', *J. Am. Chem. Soc.*, 2007, **129**, pp. 8406–8407
[24] Chandra R., Mukhopadhyay S., Nath M. 'Tio_2@ZIF-8: a novel approach of modifying micro-environment for enhanced photocatalytic dye degradation and high usability of TiO_2 nanoparticles', *Mater. Lett.*, 2016, **164**, pp. 571–574
[25] Ye L.Q., Liu J.Y., Gong C.Q., *ET AL.*: 'Two different roles of metallic Ag on Ag/Agx/BiO*X* (*X* = Cl, Br) visible-light photocatalysts: surface plasmon resonance and *Z*-scheme bridge', *ACS Catal.*, 2012, **2**, (8), pp. 1677–1683
[26] Jiang G.H., Tang B.L., Li X., *ET AL.*: 'Preparation of Ag-modified Zn_2GeO_4 nanorods for photodegradation of organic pollutants', *Powder Technol.*, 2014, **251**, pp. 37–40
[27] Zhang X., Ai Z.H., Jia F.L., *ET AL.*: 'Generalized one-pot synthesis, characterization, and photocatalytic activity of hierarchical BiO*X* (*X* = Cl, Br, I) nanoplate microspheres', *J. Phys. Chem. C*, 2008, **112**, (3), pp. 747–753
[28] Chen E.C.M., Wentworth W.E., Ayala J.A. 'The relationship between the Mulliken electronegativities of the elements and the work functions of metals and non-metals', *J. Chem. Phys.*, 1977, **67**, (6), pp. 2642–2647

© The Institution of Engineering and Technology 2020